The impact of high frequency rapid viral antigen screening on COVID-19 spread and outcomes: a validation and modeling study

Authors: Beatrice Nash[1,2*], Anthony Badea[1,3*], Ankita Reddy[1,4*], Miguel Bosch[1,5], Nol Salcedo[1], Adam R. Gomez[1], Alice Versiani[6], Gislaine Celestino Dutra Silva[6], Thayza Maria Izabel Lopes dos Santos[6], Bruno H. G. A. Milhim[6], Marilia M Moraes[6], Guilherme Rodrigues Fernandes Campos[6], Flávia Quieroz[6], Andreia Francesli Negri Reis[6], Mauricio L. Nogueira[6], Elena N. Naumova[7], Irene Bosch[1,8], Bobby Brooke Herrera[1,9†]

[*]These authors contributed equally to this work.

Affiliations:

[1]E25Bio, Inc., Cambridge, MA, USA

[2]Department of Computer Science, Harvard University School of Engineering and Applied Sciences, Cambridge, MA, USA

[3]Department of Physics, Harvard University, Cambridge, MA, USA

[4]Perelman School of Medicine, University of Pennsylvania, Philadelphia, PA, USA

[5]InfoGeosciences LLC, Houston, TX, USA

[6]Faculdade de Medicina de São José do Rio Preto (FAMERP), São José do Rio Preto, Brazil

[7]Division of the Nutrition Epidemiology and Data Science, Friedman School of Nutrition Science and Policy, Tufts University, Boston, MA, USA

[8]Department of Medicine, Mount Sinai School of Medicine, New York, NY, USA

[9]Department of Immunology and Infectious Diseases, Harvard T.H. Chan School of Public Health, Boston, MA, USA

†Corresponding Author. BBH, email: bbherrera@e25bio.com

Abstract

High frequency screening of populations has been proposed as a strategy in facilitating control of the COVID-19 pandemic. Here we use computational modeling, coupled with clinical data from a rapid antigen test, to predict the impact of frequent rapid testing on COVID-19 spread and outcomes. Using patient nasopharyngeal or nasal swab specimens, we demonstrate that the sensitivity/specificity of two rapid antigen tests compared to quantitative real-time polymerase chain reaction (qRT-PCR) are 80.0%/91.1% and 84.7%/85.7%, respectively; moreover, sensitivity correlates directly with viral load. Based on COVID-19 data from three regions in the United States and São José do Rio Preto, Brazil, we show that high frequency, strategic population-wide rapid testing, even at varied accuracy levels, diminishes COVID-19 infections, hospitalizations, and deaths at a fraction of the cost of nucleic acid detection via qRT-PCR. We propose large-scale antigen-based surveillance as a viable strategy to control SARS-CoV-2 spread and to enable societal re-opening.

INTRODUCTION

The COVID-19 pandemic has taken an unprecedented toll on lives, wellbeing, healthcare systems, and global economies. As of 25 September 2020, there have been more than 32.1 million confirmed cases globally with more than 980,000 confirmed deaths (*1*). However, these numbers and the current mapping of disease spread present an incomplete picture of the outbreak largely due to the lack of adequate testing, particularly as undetected infected cases are the main source of disease spread (*2–7*). It is estimated that the reported detection rate of actual COVID-19 cases is only 1-2% (*5*). As of September 2020, the United States and Brazil remain the top two countries with the highest number of COVID-19 cases and deaths worldwide. As countries begin to re-open their economies, a method for accessible and frequent surveillance of COVID-19, with the necessary rapid quarantine measures, is crucial to prevent the multiple resurgences of the disease.

The current standard of care rightfully places a strong focus on the diagnostic limit of detection, yet frequently at the expense of both cost and turnaround time. This situation has contributed to limited population testing largely due to a dearth of diagnostic resources. Quantitative real-time polymerase chain reaction (qRT-PCR) is the gold-standard method for clinical diagnosis, with high sensitivity and specificity, but these tests are accompanied by the need for trained personnel, expensive reagents and instrumentation, and a significant amount of time to execute. Facilities offering qRT-PCR sometimes require a week or longer to complete and return the results to the patient. During this waiting period the undiagnosed individual may spread the infection and/or receive delayed medical treatment. Moreover, due to the cost and relative inaccessibility of qRT-PCR in both resource-limited and abundant settings, large-scale screening using qRT-PCR at frequent intervals remains impractical to identify infected but asymptomatic or mildly symptomatic infections. Numerous studies have reported asymptomatic COVID-19 cases

92 as well as a variation in viral load within and between individuals at different time points,
93 suggesting the need for more frequent testing for informative surveillance.

94 Technologies alternate to qRT-PCR, such as rapid viral antigen detection, clustered
95 regularly interspaced short palindromic repeats (CRISPR), and loop-mediated isothermal
96 amplification (LAMP) of SARS-CoV-2 provide potential large-scale screening applications, yet
97 their implementation is stymied by requirements for qRT-PCR-like accuracy before they can reach
98 the market (*8*). In countries such as India, where the qRT-PCR resources would not be sufficient
99 to cover monitoring of the population, the use of rapid antigen tests is well underway(*9*, *10*). In
100 early May 2020, the United States Food and Drug Administration (FDA) authorized the first
101 antigen test for the laboratory detection of COVID-19, citing a need for testing beyond molecular
102 and serological methods. Antigen testing detects the viral proteins rather than nucleic acids or
103 human antibodies, allowing for detection of an active infection with relative ease of sample
104 collection and assay. These rapid assays – like other commercially-available rapid antigen tests -
105 can be mass-produced at low prices and be administered by the average person without a laboratory
106 or instrumentation. These tests also take as little as 15 minutes to determine the result, enabling
107 real-time surveillance and/or diagnosis. Although antigen tests usually perform with high
108 specificities (true negative rate), their sensitivity (true positive rate) is often lower when compared
109 to molecular assays. While qRT-PCR can reach a limit of detection as low as 10^2 genome copies
110 per mL, rapid antigen testing detects viral protein that is assumed to correlate with approximately
111 10^5 genome copies per mL (*11*).

112 We hypothesize that frequent antigen-based rapid testing even with lower sensitivities
113 compared to qRT-PCR - along with appropriate quarantine measures - can be more effective at
114 decreasing COVID-19 spread than less frequent molecular testing of symptomatic individuals.

115 Keeping in mind the realities of daily testing in resource-limited regions, we also hypothesize that
116 testing frequency can be adjusted according to the prevalence of the disease; that is, an uptick in
117 reported cases should be accompanied by more frequent testing. During the viral incubation period,
118 high infectivity correlates with a high viral load that can be detected by either qRT-PCR or rapid
119 antigen testing (*12–16*). Rapid tests thus optimize diagnosis for the most infectious individuals.
120 Studies also point to the relatively small window of time during an individual's incubation period
121 in which the qRT-PCR assay is more sensitive than rapid tests (*12*).

122 In this study we report the clinical validation of two direct antigen rapid tests for detection
123 of SARS-CoV-2 spike glycoprotein (S) or nucleocapsid protein (N) using retrospectively collected
124 nasopharyngeal or nasal swab specimens. Using the clinical performance data, we develop a
125 modeling system to evaluate the impact of frequent rapid testing on COVID-19 spread and
126 outcomes using a variation of a SIR model, which has been previously used to model COVID-19
127 transmission (*17–23*). We build on this model to incorporate quarantine states and testing protocols
128 to examine the effects of different testing regimes. This model distinguishes between undetected
129 and detected infections and separates severe cases, specifically, those requiring hospitalization,
130 from those less so, which is important for disease response systems such as intensive care unit
131 triaging. We simulate COVID-19 spread with rapid testing and model disease outcomes in three
132 regions in the United States and São José do Rio Preto, Brazil - the site of the clinical validation
133 study - using publicly available data. To date, COVID-19 modeling describes the course of disease
134 spread in response to social distancing and quarantine measures, and a previous simulation study
135 has shown that frequent testing with accuracies less than qRT-PCR, coupled with quarantine
136 process and social distancing, are predicted to significantly decrease infections (*12*, *17*, *23–27*).
137 This is the first modeling system using publicly-available data to simulate how potential public

138 health strategies based on testing performance, frequency, and geography impact the course of
139 COVID-19 spread and outcomes. Our findings suggest that a rapid test, even with sensitivities
140 lower than molecular tests, when strategically administered 2-3 times per week, will reduce
141 COVID-19 spread, hospitalizations, and deaths at a fraction of the cost of nucleic acid testing via
142 qRT-PCR. Modern surveillance systems should be well equipped with rapid testing tools to ensure
143 that disease tracking and control protocols are effective and well-tailored to national, regional, and
144 community needs.
145
146 **RESULTS**
147 **Accuracy of Direct Antigen Rapid Tests Correlate with Viral Load Levels**
148 Rapid antigen tests have recently been considered a viable source for first-line screening,
149 although concerns about the accuracy of these tests persist. We clinically validated two different
150 direct antigen rapid tests for the detection of either N or S from SARS-CoV-2 in retrospectively
151 collected nasal or nasopharyngeal swab specimens. Of the total number of nasal swab specimens
152 evaluated by qRT-PCR for amplification of SARS-CoV-2 N, S, and ORF1ab genes, 100 tested
153 positive and 90 tested negative (Table 1, Table S1). The overall sensitivity and specificity of the
154 rapid antigen test for detection of SARS-CoV-2 N, evaluated across the nasal swab specimens,
155 was 80.0% and 91.1%, respectively. Of the total number of nasopharyngeal swab specimens
156 evaluated by qRT-PCR for amplification of SARS-CoV-2 N, RNA-dependent RNA polymerase
157 (RdRp), and envelope (E) genes, 72 tested positive and 49 tested negative (Table 2, Table S1). The
158 overall sensitivity and specificity of the rapid antigen test for detection of SARS-CoV-2 S,
159 evaluated across the nasopharyngeal swab specimens was 84.7% and 85.7%, respectively.

160 Altogether, our data demonstrate that the sensitivity of the rapid antigen tests are positively
161 correlated to the viral load level (Table S1).

162 The Ct value indirectly quantifies the viral RNA copy number related to the viral load of
163 the sample for the specific assay (*28*, *29*). Ct values represent the number of qRT-PCR cycles at
164 which generated fluorescence crosses a threshold during the linear amplification phase; Ct values
165 are therefore inversely related to the viral load. Notably, the sensitivity of both rapid antigen tests
166 increases as Ct value decreases (Table S1). The sensitivity of the rapid antigen test for detection
167 of SARS-CoV-2 N increased from 80.0% at Ct values <40 to 95.8% at Ct values <20. Similarly,
168 the sensitivity of the rapid antigen test for detection of SARS-CoV-2 S increased from 84.7% at
169 Ct values <35 to 100.0% at Ct values <15. Taken together, the clinical data shows that the rapid
170 antigen test performs with increasing accuracy for individuals with a higher viral load, and
171 potentially the most infectious (*13–16*).

172

173 **An Enhanced Epidemiological SIDHRE-Q Model**

174 We propose an enhanced epidemiological modeling system, *SIDHRE-Q,* a variant of the
175 classical SIR model in order to expand our clinical validation study and to understand the effects
176 of using frequent rapid tests such as the rapid antigen test on COVID-19 outbreak dynamics. The
177 changes we make to the basic model to encompass the unique characteristics of the COVID-19
178 pandemic are similar to those presented by Giordano et al. *(16)* (Figure 1, Figure S1). The
179 differential equations governing the evolution of the *SIDHRE-Q* model and descriptions of the
180 parameter values are provided in the material and methods section (Equation 2, Table 3).

181 An individual that begins in **S** may either transition to a Quarantine Uninfected (**Q-U**) state
182 via a false positive result or to an Infected Undetected (**I**) state via interaction with an infected

individual. Should an individual in **S** move into **Q-U**, they are quarantined for 14 days before returning to **S**, a time period chosen based on current knowledge of the infectious period of the disease. One could also conceive of an effective strategy in which individuals exit quarantine after producing a certain number of negative rapid tests in the days following their initial positive result or confirm their negative result using qRT-PCR.

Given that those diagnosed are predominantly quarantined, individuals in **I** interact more with the **S** population than do those in Infected Detected (**D**). Therefore, the infectious rate for **I** is assumed to be significantly larger than for **D**. Furthermore, a region's ability to control an outbreak is directly related to how quickly and effectively people in **I** test into **D**, reducing their infectiousness through quarantine. This study, in particular, highlights the critical role frequency of testing, along with strict quarantine, has in mitigating the spread of the disease and provides specific testing strategies based on rapid tests we predict to be highly effective.

In this model, we assume that individuals receive a positive diagnosis before developing severe symptoms and that those with symptoms severe enough to be potentially fatal will go to the hospital. If an individual develops symptoms, we assume they are tested daily until receiving a positive result; hence, before severe symptoms develop, they will be diagnosed with high probability. Those who do not develop symptoms are tested according to the frequency of tests administered to the general population. Therefore, there is no modeled connection between **I** and **H** or between **I** and **E**. Removing these assumptions would have negligible impact on the results as these flows are very small.

Should an individual test positive and transition to **D**, they may either develop serious symptoms requiring care or recover. Those who develop serious symptoms and transition to state **H** will then transition to either **R** or **E**. The recovered population is inevitably tested, as infected

individuals may recover without being detected. Therefore, the Quarantined Recovered (**Q-R**) state is introduced with the same connections to **R** as the connections between **S** and **Q-U**. Though the reinfection rate of SARS-CoV-2 has been a point of recent debate, it is assumed that the number of re-infected individuals is small (*30–34*). Therefore, individuals cannot transition from **R** to **S**, hence the separately categorized quarantined populations.

We considered several variations and extensions of the *SIDHRE-Q* model. In simulations, we tested additional states, such as those in the *SIDARTHE* model, which include distinctions between symptomatic and asymptomatic cases for both detected and undetected populations (*17*). Incorporating information about the correlations between viral load and infectivity and sensitivity were also considered. Altogether, our modeling system has been well tuned to predict the impact of high frequency rapid testing on COVID-19 spread and outcomes.

Frequent Rapid Testing with Actionable Quarantining Dramatically Reduces Disease Spread

In order to demonstrate how strategies could affect the disease spread in different geographies and demographics, we used surveillance data obtained from regions of varying characteristics: the state of Massachusetts (MA), New York City (NYC), Los Angeles (LA), and São José do Rio Preto (SJRP), Brazil, the site of the rapid antigen test clinical validation study. These regions are also selected in our study due to the readily available surveillance data provided by the local governments. We fit the model to the data from each region starting 1 April 2020. At this time point the disease reportedly is most advanced in NYC and least advanced in SJRP, Brazil with estimated cumulative infection rates of 7.11% and 0.12%, respectively.

228 After calibrating the *SIDHRE-Q* model, the disease spread is observed with varying
229 validated rapid antigen test performances and frequencies (Figure 2A). Sensitivity (the ratio of true
230 positives to the total number of positives) and specificity (the ratio of true negatives to the total
231 number of negatives) compared to gold-standard qRT-PCR were used as measures of test
232 accuracy.

233 The rapid test frequency is varied while maintaining an accuracy of 80% sensitivity and
234 90% specificity, comparable to our clinical data collected in SJRP, Brazil. These testing scenarios
235 are then compared to symptomatic testing, in which individuals receive a rapid test only when
236 presenting symptoms, via either a rapid test or qRT-PCR. Since the primary testing regiment
237 deployed in MA, LA, NYC and SJRP, Brazil is qRT-PCR-based and focused on symptomatic
238 individuals, the symptomatic testing protocol via qRT-PCR is directly estimated from the data to
239 be the rate ν (Table 3).

240 The difference between the qRT-PCR and rapid test simulations (red and orange lines,
241 respectively) is therefore only sensitivity of testing (Figure 2A). We assumed that test outcome
242 probability is a function only of whether an individual is infected and independent of other factors;
243 one can consider this a lower bound on effectiveness of a strategy, as sensitivity and infectivity
244 are often positively correlated with antigen testing.

245 To better understand the effect of rapid testing frequency and performance on healthcare
246 capacity and mortality rates, we simulate the testing strategy with 30%-90% sensitivity each with
247 80% or 90% specificity against the symptomatic testing strategy (Figure S2).

248 As per our hypothesis, frequency and symptom-based testing dramatically reduced
249 infections, simultaneous hospitalizations, and total deaths when compared to the purely symptom-
250 based testing regiments, and infections, hospitalization, and death were reduced as frequency

251 increased. Although testing every day was clearly most effective, even testing every fourteen days
252 with an imperfect test gave an improvement over symptomatic testing with qRT-PCR. While the
253 strategy works best when implemented at the very beginning of an outbreak, as demonstrated by
254 the results in SJRP, Brazil, it also works to curb an outbreak that is already large, as demonstrated
255 by the results in NYC. The difference between frequencies is more noticeable when the testing
256 strategy is applied to the outbreak in NYC, leading us to hypothesize that smaller outbreaks require
257 a lower testing frequency than larger ones; note the difference between the dependence on
258 frequency to curb a small initial outbreak in SJRP, Brazil versus a large one in NYC (Figure 2B).

259 For test performance of 80% sensitivity and 90% specificity, the percent of the population
260 that has been infected in total from the beginning of the outbreak to mid-July drops from 18%
261 (MA), 11% (LA), 26% (NYC), and 11% (SJRP, Brazil) to 3%, 2%, 12%, and 0.26%, respectively,
262 using a weekly rapid testing and quarantine strategy (with regards to predictions of overall
263 infection rates, other studies based on seroprevalence and epidemiological predictions have
264 reached similar conclusions (*35*, *36*)). If testing is increased to once every three days, these
265 numbers drop further to 1.6% (MA), 1.4% (LA), 9.4% (NYC), and 0.19% (SJRP, Brazil) (Table
266 S2).

267 To further examine the relationship between frequency and sensitivity, we modeled the
268 maximum number of individuals in a given state over the 105-day time period for four geographic
269 regions (Figure 2B, Figure S3). In all four geographic regions, as frequency of testing increases,
270 the total infections, maximum simultaneous hospitalizations, and total deaths converge to small
271 percentages regardless of the sensitivity at high frequencies. It is clear that the difference in
272 frequency required to achieve the same result using tests of differing sensitivities is very small.
273 For example, we predict that for the outbreak in LA, a testing strategy started on 1 April of every

10 days using a test of sensitivity 90% would have resulted in 2.5% of the population having been infected, while using a test of sensitivity 30% would require a strategy of every 5 days to achieve the same number. Thus, we conclude that frequency is more important than sensitivity in curbing the spread, and a large range of sensitivities prove effective when testing sufficiently often (Figure S3). How frequently, exactly, depends on the specific outbreak and what stage it is in, which leads us to the location-based deployment strategy discussed in a later section. Frequency of testing can be significantly reduced to effectively contain the disease once the initial outbreak has been controlled; it is clear that this takes only a matter of weeks (Figure 2A).

On the other hand, according to the specificity of the rapid test and the quarantine duration, larger testing frequency result in a larger percent of the population quarantined (Figure 2A). Assuming a 90% rapid test specificity and 14-day quarantine duration, for the 1-, 3- and 7-day frequencies almost 60%, 38% and 20% of the population, respectively, would be quarantined. This figure may be reduced with additional rules for exiting quarantine early, such as after complementary testing. An example of such a strategy is that individuals who test positive are required to either quarantine for two weeks or produce two consecutive negative rapid tests in the two days following their positive result. Assuming 80% sensitivity and 90% specificity, those individuals will reenter the public while still infected with probability 0.04. If uninfected, that individual will exit quarantine after two days with probability 0.81. However, a compromise between the reduction of infections and the proportion of the population in quarantine would be part of the planning for the appropriate testing protocol in each community or region.

Additionally, while high frequency may be necessary to contain a large outbreak initially, relatively infrequent testing, such as every one or two weeks, is sufficient to keep controlled

outbreaks small, while reducing the number of quarantined individuals to less than 10% of the population using a two-week mandatory quarantine.

A County-Based Testing Strategy Offers a Cost-effective Approach to Large-scale COVID-19 Surveillance

To examine the effects of resource-strategic testing schemes, we modeled the COVID-19 prevalence by varying testing frequency across counties of California. For this analysis, only California was analyzed because of the accessibility of the county level data. In this scheme, the percent of active infected detected individuals in a county determines the frequency of testing. We define thresholds for the number of active detected infections that, when hit, initiate testing protocols of different frequencies depending on the threshold hit. We first tested evenly spaced thresholds for the number of detected active infections up to 1% of the population, but later adopted thresholds that were determined according to Equation 1. In Equation 1, D = population of state **D** at the time of testing. T = number of active infections which, if reached, initiates everyday testing. The days between tests are rounded to the closest integer value.

$$\text{Days between tests} = \max\left(1, 2\log_2(T/D) + 1\right) \tag{1}$$

The days between tests are chosen such that the detected active infections should remain near to or below T. If the initial detected active infections are greater than T, then the testing frequency of 1 will cause infections to rapidly drop. Both the threshold at which everyday testing begins and the coefficient of $log_2 T/D$ can be modified to produce a strategy that is more or less frequent in testing or resource effective; a range of days between tests from 14 days to 1 day are used (Figure 3). A scan over different choices of T is shown in Figures S5 and S6; the threshold

319 we choose in Figure 3 is 0.05% because it is successful in curbing the outbreak within the time
320 period we consider. While these choices work for the epidemic in California at the point we start
321 our simulations, 10 April, they do not necessarily reflect the most resource effective choices
322 everywhere. Our analysis could be redone to select the best strategy in other states or in the country
323 as a whole.

324 Using a rapid test with a sensitivity of 80% and specificity of 90%, the county-based testing
325 with threshold 0.05% reduces the active infections from 0.94% to 0.0005%, while the uniform
326 strategy with tests administered every 7 days results in double the number of active infections
327 (Figure 3). As the threshold is reduced, the total cost increases while the cumulative infections,
328 maximum percentage hospitalized, and cumulative deaths all decrease (Figure S4).

329 Strategy B in Figure 3 consists of qRT-PCR testing uniformly applied to the highlighted
330 population with a frequency of once weekly. The average cost per person per day is just under $15.
331 Despite this frequency and the accuracy of qRT-PCR, the strategy does not succeed in curbing the
332 spread as fast as strategy A, which uses a testing sensitivity and specificity of 80% and 90%,
333 respectively, and testing frequency that vary between counties depending on the proportion of their
334 population that is currently infected. The total cost for strategy A is estimated at a fraction of the
335 other at $1.53 per person per day.

336

337

338 **DISCUSSION**

339 In this study we examine the potential effects of a novel testing strategy to limit the spread
340 of SARS-CoV-2 utilizing rapid antigen test screening approaches. Our clinical data and *SIDHRE-*
341 *Q* modeling system demonstrate that 1) frequent rapid testing even at a range of accuracies is
342 effective at reducing COVID-19 spread, 2) rapid antigen tests are a viable source for this strategy

343 and diagnose the most infectious individuals, and 3) strategic geographic-based testing can
344 optimize disease control with the amount of available resources. The information from a diagnostic
345 test itself is of tremendous value, as it can prompt the necessary quarantine measures to prevent
346 spread, guide proper care and triage, and provide crucial disease-tracking information. Diagnostic
347 testing in the United States and abroad, however, has been a significant public health hurdle. The
348 public has witnessed and experienced symptomatic individuals being denied testing due to
349 shortages, and few testing structures for asymptomatic or mildly symptomatic individuals – a
350 significant source of disease spread. Though several factors contributed to the stymied early
351 response measures, such as lockdown and quarantine protocols and adherence, severe testing
352 bottlenecks were a significant culprit (*37–39*). Early control measures have been shown to decrease
353 lives lost by several orders of magnitude (*40*). These challenges, though exacerbated during the
354 early months of the pandemic, remain at the forefront of the public health crises.

355 Diagnosis of SARS-CoV-2 infection by qRT-PCR is the current standard of care, yet
356 remains expensive and requires a laboratory and experienced personnel for sample preparations
357 and experimentation. Significantly, the turnaround time for results can be up to 10 days (*41*). On
358 an individual scale, this leaves the public in limbo, preventing people from either leaving
359 quarantine if they are negative, or delaying critical care and infecting others if they are positive.
360 On a societal level, this current testing scheme yields incomplete surveillance data on which
361 response efforts such as societal reopening and hospital management depend. Though qRT-PCR
362 is considered the gold-standard diagnostic method because of its high sensitivity and specificity,
363 the logistical hurdles render it unrealistic for large-scale screening.

364 As qRT-PCR remains impractical for this strategy, and rapid tests are facing regulatory
365 challenges because they do not perform with qRT-PCR-like accuracy, rapid test screening is either

366 nonexistent in several countries or symptom-based. Even under best-case assumptions, findings
367 have shown that symptom and risk-based screening strategies miss more than half of the infected
368 individuals (*42*). Some have argued that the need for widespread testing is overstated due to the
369 variability in test sensitivity and specificity (*43*). Here, we present alternative large-scale
370 diagnostic tools to qRT-PCR, and show that test performance, though valuable, is secondary to
371 widespread test frequency, which is enabled by accessibility and turnaround time. Furthermore,
372 test affordability is essential for the successful implementation in communities most affected by
373 infection and will to speed up the safe opening and functioning of the viral sectors of the economy.
374 Giordano et al. has modeled the evolution of SARS-CoV-2 spread, introducing a diagnosed
375 state to elucidate the importance of population-wide testing (*17*). Mina et al. has examined how
376 various test sensitivities and frequencies affect the reproductive number (*12*). We build upon these
377 findings to show how in affected United States and Brazil regions, population-wide frequent and
378 rapid testing schemes, with sensitivities ranging from 30%-90%, can be more effective in curbing
379 the pandemic than a PCR-based scheme. Integrating real-world surveillance and clinical data into
380 our modeling system has allowed us to incorporate regional differences - such as variances in
381 healthcare access, state health policy and adherence, state GDP, and environmental factors - under
382 the same model. Significantly, our findings hold true across Massachusetts, New York City, Los
383 Angeles, and São José do Rio Preto, Brazil. We also present the economic considerations of these
384 testing regimes, showing that widespread rapid testing is more cost efficient than less frequent
385 qRT-PCR testing. In line with these economic considerations, our model demonstrates the
386 effectiveness of a geographic-based frequent testing regime, in which high disease prevalence
387 areas receive more frequent testing than low disease prevalence areas.

388 Since COVID-19 is known to affect certain demographics differently, modeling would
389 benefit from incorporating demographic information correlated with disease progression and
390 spread to define sub-models and sets of parameters accordingly. Age, pre-existing conditions, job
391 types, and density of population are examples of possible categories, each of which influence the
392 risk of contracting and/or dying from COVID-19. Further studies would benefit from incorporating
393 these ideas to better understand the effectiveness of rapid testing on identifying potential super
394 spreading events. Future public health prevention programs should use the proposed modeling
395 system to develop and test scenarios for precision testing and prevention.

396 Our findings also point to low-cost tools for implementation of this testing strategy, such
397 as a rapid antigen-based test for the detection of SARS-CoV-2 proteins. We show that the rapid
398 antigen tests perform with a range of accuracies under which disease spread can be dramatically
399 mitigated under our model. Notably, the sensitivity is correlated to the individual's viral load,
400 effectively diagnosing those who are potentially the most infectious with the highest accuracy. Our
401 findings are significant because rapid antigen tests are cheaper than qRT-PCR, can be mass
402 produced to millions per day, present results within 15 minutes, and can be administered by a
403 nonexpert without a lab or special equipment.

404 There are several policy implications for these findings. First, our model supports that
405 systems of high frequency rapid testing should be implemented as a first-line screening method.
406 This can be first enabled by a more holistic regulatory evaluation of rapid diagnostics, such that
407 policy emphasizes accessibility and turnaround time even under a range of accuracies. One can
408 imagine a less accurate, though rapid method of first-line screening in schools, public
409 transportation, and airports, or even at home, and a qRT-PCR-based method for second-line
410 screening (testing those who present severe symptoms or have been in contact with infected

411 individuals, testing in a clinical setting, etc). Second, our cost analysis and rapid antigen test data
412 present a viable and potentially more cost-effective method for screening. Third, our county-based
413 testing scheme presents a possible method for wide-scale screening while optimizing resources.
414 Future studies should investigate how this selective testing strategy can be applied to different
415 location scales to further inform health policy. Moreover, though our models analyze regions in
416 the United States and Brazil, similar testing strategies can be considered globally in both resource
417 limited and abundant settings due to the higher accessibility of rapid tests compared to qRT-PCR.

418 We emphasize that integral to the effectiveness of diagnostic schemes is 1) the proper
419 adherence to quarantine measures and 2) the combined use of a variety of diagnostic methods
420 including nucleic acid, antigen, and antibody tests. According to these models, rapid antigen tests
421 are an ideal tool for first-line screening. Clinical molecular tests such as qRT-PCR are vital to the
422 diagnostic landscape, particularly to re-test suspected cases that were negative on the rapid test.
423 Because rapid tests present a higher rate of false negatives, methods such as qRT-PCR remain
424 integral to second-line screening. Antibody tests provide important information for immunity and
425 vaccination purposes as well as epidemiological surveillance. This model also assumes that
426 individuals will quarantine themselves before being tested and for 14 days following a positive
427 diagnostic result.

428 Our simulations combined with real-world data demonstrate a robust modeling system and
429 elucidates the significance of this novel testing strategy. However, there are important limitations
430 to be considered. Differences in disease reporting between the geographical regions and the
431 incomplete nature of COVID-19 surveillance data, often due to the lack of testing, are not
432 considered in the model. It is imperative that the testing results, hospitalization and death statistics,
433 and changes in protocol are reported in real-time to scientists and policy makers so that models

434 can be accurately tuned as the pandemic develops. The model also does not take into account
435 infrastructural limitations such as hospital capacity. Though the rapid antigen test offers several
436 advantages such as affordability, fast turnaround time, and ease of mass production, we are also
437 assuming that there are systems in place to implement frequent and safe low-cost screening across
438 different communities and settings.

439 Our model underscores the need for a point-of-care or at-home test for frequent screening,
440 particularly as lockdown restrictions ease. Regulatory agencies such as the FDA could work
441 towards regulating rapid tests to alternative standards other than comparison to high sensitivity
442 molecular diagnostics, as our model shows that frequency and scale of testing may overcome lower
443 sensitivities. Rather, we could refocus policy to implement first-line screening that optimizes
444 accuracy with efficiency and equitability.

445

446 **MATERIAL AND METHODS**

447 **Development of Direct Antigen Rapid Tests for the Detection of SARS-CoV-2**

448 We developed a direct antigen rapid test for the detection of the nucleocapsid protein or
449 spike glycoprotein from SARS-CoV-2 in nasal or nasopharyngeal swab specimens as previously
450 described (*44*). Briefly, the rapid antigen tests are immunochromatographic format with a visual
451 readout using anti-N or anti-S mouse monoclonal antibodies (E25Bio, Inc., Cambridge, MA, USA)
452 that are either coupled to 40 nm gold nanoparticles (Abcam, Cambridge, UK) or adsorbed to
453 nitrocellulose membranes (Sartorius, Goettingen, Germany). Each rapid antigen test has a control
454 area adjacent to the paper absorbent pad; the control is an anti-mouse Fc domain antibody (Leinco
455 Technologies, Fenton, MO, USA) that will capture any of the antibody-conjugated gold
456 nanoparticles to generate a control visual signal. A visual signal at the test area reflects SARS-

457 CoV-2 N or S that is "sandwiched" between an anti-N or anti-S antibody adsorbed to the
458 nitrocellulose membrane and a second anti-N or anti-S antibody covalently coupled to visible gold
459 nanoparticles.
460
461 **Validation of Direct Antigen Rapid Test for the Detection of SARS-CoV-2**
462 In a retrospective study of nasal swab specimens form human patients, we compared the
463 accuracy of the rapid antigen test for detection of SARS-CoV-2 N to the viral loads of individuals.
464 Nasal swab specimens (n=190) were tested following approved human subjects use protocols. The
465 nasal swab specimens were banked frozen from suspected patients submitted to PATH for routine
466 COVID diagnosis. Prior to using the rapid test, the nasal swab specimens were validated by qRT-
467 PCR using the FDA EUA ThermoFisher/AppliedBiosystems TaqPATH COVID-19 Combo Kit
468 (ThermoFisher, Waltham, MA USA). The primary study under which the samples and data were
469 collected received ethical clearance from the PATH Research Ethics Committee, protocol number
470 00004244. The nasal swab specimens were de-identified, containing no demographic data, prior
471 to analysis.
472 Additionally, in a retrospective study of nasopharyngeal swab specimens from human
473 patients, we compared the accuracy of the rapid antigen test to the viral load of individuals.
474 Nasopharyngeal swab specimens (n = 121) were tested in Brazil following approved human
475 subjects use protocols. The age of study participants ranged from 1 to 95 years with an overall
476 median of 37 years (interquartile range, 27–51 years), and 62% were female. The demographic
477 summary of the patients are included in Table S3. The nasopharyngeal swab specimens were
478 banked refrigerated or frozen samples from suspected patients submitted to the lab for routine
479 COVID diagnosis. Prior to using the rapid test, the nasopharyngeal swab samples were validated

480 by qRT-PCR using GeneFinder™ COVID-19 Plus Real*Amp* Kit (OSANGHealtcare, Anyang-si,
481 Gyeonggi-do, Republic of Korea I). The primary study under which the samples and data were
482 collected received ethical clearance from the Faculdade de Medicina de São José do Rio Preto
483 (FAMERP), protocol number 31588920.0.0000.5415. All excess samples and corresponding data
484 were banked and de-identified prior to the analyses.

485 A nasopharyngeal swab specimen (1 mL) was concentrated using a Vivaspin 500
486 centrifugal concentrator (Sartorius, Goettingen, Germany) at 12,000 x g for 10 minutes. The
487 concentrated nasopharyngeal swab specimen retentate was transferred to a collection tube and the
488 rapid antigen test was inserted into the tube with the retentate and allowed to react for 15 minutes.
489 After processing of the rapid antigen test, the visual positive or negative signal was documented.
490

491 **Data for Modeling**

492 As of August 2020, the United States and Brazil have the highest number of confirmed
493 COVID-19 cases and deaths worldwide, with both countries reporting their first case on 26
494 February 202) (*1*). Although several affected US regions could have been modeled, we look at
495 data from Massachusetts, New York, and Los Angeles: these regions each contained "hotspots",
496 or areas of surging COVID-19 cases, at different points in time during the pandemic and have
497 publicly available government-provided surveillance data. Our model is fit using data over 105
498 days beginning on April 1 for Figure 2 and 105 days beginning on April 10 for Figure 3 (see
499 "Modeling Parameters" in Methods). In order to understand the various testing proposals on a
500 global scale, we performed our clinical study in and expanded the modeling study to Brazil. The
501 specific data we use to fit our model are cumulative confirmed cases, total deaths, and number of

daily hospitalizations due to COVID-19. This surveillance data was retrieved from government-provided online databases (*45–51*).

Modeling Parameters

Equation 2 below provides the exact differential equations governing the model.

$$
\begin{aligned}
\mathrm{d}\mathbf{S} &= & -\mathbf{S}\left(\alpha\mathbf{I}+\eta\mathbf{D}+\gamma\right) & & +\psi\mathbf{Q_U} \\
\mathrm{d}\mathbf{I} &= & -\mathbf{I}\left(\varepsilon+\lambda+\nu\right) & & +\mathbf{S}\left(\alpha\mathbf{I}+\eta\mathbf{D}\right) \\
\mathrm{d}\mathbf{D} &= & -\mathbf{D}\left(\frac{\mathbf{D}+\mathbf{I}}{\mathbf{D}}\mu+\rho\right) & & +\mathbf{I}(\nu+\varepsilon) \\
\mathrm{d}\mathbf{H} &= & -\mathbf{H}\left(\sigma+\tau\right) & & +\mu\left(\mathbf{D}+\mathbf{I}\right) \\
\mathrm{d}\mathbf{E} &= & & & +\tau\mathbf{H} \\
\mathrm{d}\mathbf{R} &= & -\gamma\mathbf{R} & & +\rho\mathbf{D}+\lambda\mathbf{I}+\sigma\mathbf{H}+\psi\mathbf{Q_R} \\
\mathrm{d}\mathbf{Q_U} &= & -\psi\mathbf{Q_U} & & +\gamma\mathbf{S} \\
\mathrm{d}\mathbf{Q_R} &= & -\psi\mathbf{Q_R} & & +\gamma\mathbf{R}
\end{aligned}
\tag{2}
$$

In order to determine the values of the parameters defining the flows between states, we use a least squares regression performed at seven day intervals in the datasets to which we fit. This allows the model to take into account the time dependent nature of the parameters, which rely on factors such as social distancing regulations and changes in testing capacity. We also fit window sizes between 1 and 21 days and find that while the fit degrades with larger window size, the overall shape of the fits do not change. We choose seven days assuming policy changes take a week to become effective and that reasonable parameters can be expected to change within this time period. Also, the seven day window size accounts for the fact that often data is not reported as diligently over the weekend. Time series of the values of the parameters for the geographic locations discussed in this paper are included in Figure S5.

Given the restrictions on data available for the populations of various states, varying all of the parameters results in an over parameterized system. Therefore, a subset of the model parameters are fit while the others are either extracted from other sources; see Table 3.

The fitting procedure minimizes the sum of the squared residuals of the total cases, current daily hospitalizations, cumulative deaths, and percentage of total infected individuals currently hospitalized. The first three are present in the data sets while the latter is derived from the estimates of the ratio between infected undetected to infected detected individuals from the CDC Laboratory Seroprevalence Survey Data (*52*). While this ratio changes over time, the percentage of infected individuals developing severe symptoms should remain roughly constant throughout the course of the epidemic in the different locations studied.

We consider the data sets for outbreaks in MA, NYC, LA, and SJRP, Brazil (*45–50*). While each location has testing and fatality information dating back to January, hospitalization data was not included until late March (for NYC and SJRP) and April (for MA and LA). Hence we begin our fitting procedure and testing strategy on 1 April for each of the data sets; by this point, the outbreak is advanced in NYC, substantial in MA, non-negligible, but far from its peak, in LA, and in early stages in SJRP, Brazil. Starting simulations at various stages of the outbreak allows one to see the difference in results between when a testing strategy is administered.

In order to determine the effectiveness of the county-based strategy when applied to the state of California, we also fit all of the counties in California with a population greater than 1.5% of that of the entire state and with greater than zero deaths. The results do not depend on these selections, but instead suggest a practical criteria to administer limited resources. The fitting is done starting 10 April for these counties, as at this point the outbreak is sufficiently well-

documented in each to successfully model. For the county-level data we compute a seven day running average of each of the data sets to which we then fit in order to smooth out fluctuations in the data, likely due to reporting, which are more significant here than in the other data sets considered, as the county populations are smaller and hence discrepancies impact the smoothness of the data more. The fits for each of the counties can be found in Figure S6.

As one can see from Figure 1, these data sets are particularly not smooth, which indicates inefficiencies in reporting. Additionally, it is difficult to gauge their consistency within the dates provided or to compare between locations, as reporting mechanisms changed over time within the same locations. Despite this lack of consistency, our model and fitting mechanism was successful in reproducing the progress of the outbreak in each data set studied.

The authors confirm that the data supporting the findings of this study are available within the article and/or its supplementary materials; any other data will be made available upon request. Our code can be found on github: https://github.com/badeaa3/COVID19_Rapid_Testing. The code is written using python with the packages scipy, numpy, lmfit, matplotlib and plotly (*53–57*).

564 **H2: Supplementary Materials**

565

566 **Results**

567 **Table S1. Data summary of direct antigen rapid test (DART) for detection of SARS-CoV-2**
568 **nucleocapsid protein and DART for detection of SARS-CoV-2 spike glycoprotein**
569 **performance in comparison to qRT-PCR results.**

570

571 **Table S2. Summary of results of COVID-19 outcomes in 3 US Regions and Brazil as a result**
572 **of Frequent Rapid Testing Protocol using SIDHRE-Q Model.** Total Infected, Maximum
573 Hospitalized, and Total Deaths are shown for Massachusetts, Los Angeles, New York, and São
574 Jose do Rio Preto, Brazil under a qRT-PCR protocol (symptomatic testing) and a Rapid Testing
575 protocol (once every three days with test performance of 80% sensitivity and 90% specificity).

576

577 **Table S3. Demographic and clinical summary of patients evaluated by the SARS-CoV-2**
578 **Direct Antigen Rapid Test (DART).** N response, N or mean of positive, and % or standard
579 deviation for each group is presented. All samples (n=131) collected and tested in São José do
580 Rio Preto, Brazil.

581

582 **Figure S1. Graphical scheme displaying the relationships between the stages of quarantine**
583 **and infection in *SIDHRE-Q* model: Q-U**, quarantine uninfected; **S**, susceptible (uninfected); **I**,
584 infected undetected (pre-testing and infected); **D**, infected detected (infection diagnosis through
585 testing); **H**, hospitalized (infected with life threatening symptom progression); **R**, recovered

586 (healed); **E**, extinct (dead); and **Q-R**, quarantine recovered (healed but in quarantine by false
587 positive testing).
588
589 **Figure S2. COVID-19 Outcomes as a result of Frequent Rapid Testing Protocol with**
590 **variable test performances using *SIDHRE-Q* Model.** The Cumulative Detected Infected,
591 Hospitalized, Deceased, Active Infections, Recovered, and Quarantined are modeled over 105
592 days (top to bottom) using reported data from 4 global regions: Massachusetts, Los Angeles,
593 New York City, and São José do Rio Preto in Brazil (left to right). The COVID-19 population
594 spread and outcomes are modeled under a Rapid Testing Protocol with variable testing
595 frequencies ranging from 1-21 days between tests, and variable test performances: 90%
596 specificity with 90% sensitivity (A), 70% sensitivity (B), 50% sensitivity (C), and 30%
597 sensitivity (D); and 80% specificity with 90% sensitivity (E), 70% sensitivity (F), 50%
598 sensitivity (G), and 30% sensitivity (H). This protocol is compared to a symptom-based Rapid
599 Testing protocol and a symptom-based qRT-PCR protocol.
600
601 **Figure S3. Effect of Rapid Testing Protocol under variable testing sensitivities and**
602 **increasing frequency under the *SIDHRE-Q* Model.** The Cumulative Infections, Maximum
603 Simultaneously Hospitalized, and Deceased populations are modeled for Massachusetts, Los
604 Angeles, New York City, and São José do Rio Preto in Brazil. The effect of increasing frequency
605 of testing is modeled for various testing sensitivities (30%-90%) with an 80% specificity.
606
607 **Figure S4. Effect of County Based Rapid Testing strategy on COVID-19 outcomes in**
608 **California.** This protocol varies testing frequency in accordance to the number of recorded

cases; the threshold for number of active infections which, if reached, signals to commence everyday testing, the highest frequency considered. A Rapid Test with a 80% sensitivity and 90% sensitivity is used in this deployment strategy. Shown is the total cost per person per day versus the cumulative infections, maximum simultaneously hospitalized, and cumulative deaths with varied thresholds for all of CA is shown. The County Based Rapid Testing strategy is compared to uniform testing, which distributes the same number of total tests used in the county strategy, albeit evenly across each county. The effects of uniform testing are modeled for both a Rapid Testing protocol and a qRT-PCR protocol.

Figure S5. **Time series of the four fitted parameters α, ν, μ, and τ (left to right) for MA, LA, NYC, and SJRP (top to bottom).** See Table 2 in the Methods section for an explanation of the parameters. The values are extracted every seven days from data provided by the respective regions. The parameters vary significantly over time and location. Flat points occur during the seven day windows where the parameters are held constant. The fitting procedure is also outlined in the Methods section.

Figure S6. Time series of the three fitted pieces of data Cumulative Cases, Daily Hospitalized, and Cumulative Deaths (left to right) for each county receiving testing in CA; Ventura (2A), Stanislaus (2B), Santa Clara (2C), San Joaquin (2D), San Francisco (2E), San Diego (2F), San Bernardino (2G), Sacramento (2H), Orange (2I), Los Angeles (2J), Kern (2K), Fresno (2L), Alameda (2M). The counties included satisfy two requirements: population greater than 1.5% of the total CA population and nonzero total number of deaths at each point in time. The fitting procedure is outlined in the Methods section.

632 **References and Notes**

633 1. Coronavirus Disease (COVID-19) Situation Reports, (available at
634 https://www.who.int/emergencies/diseases/novel-coronavirus-2019/situation-reports).

635 2. T. F. Menkir, T. Chin, J. A. Hay, E. Surface, P. Martinez de Salazar, C. Buckee, M. J. Mina, K. Khan, A.
636 Watts, M. Lipsitch, R. Niehus, Estimating the number of undetected COVID-19 cases exported internationally
637 from all of China. *medRxiv* (2020), doi:10.1101/2020.03.23.20038331.

638 3. B. Ivorra, M. R. Ferrández, M. Vela-Pérez, A. M. Ramos, Mathematical modeling of the spread of the
639 coronavirus disease 2019 (COVID-19) taking into account the undetected infections. The case of China.
640 *Commun Nonlinear Sci Numer Simul*, 105303 (2020).

641 4. M. Salathé, C. L. Althaus, R. Neher, S. Stringhini, E. Hodcroft, J. Fellay, M. Zwahlen, G. Senti, M. Battegay,
642 A. Wilder-Smith, I. Eckerle, M. Egger, N. Low, COVID-19 epidemic in Switzerland: on the importance of
643 testing, contact tracing and isolation. *Swiss Med Wkly*. **150**, w20225 (2020).

644 5. H. Lau, T. Khosrawipour, P. Kocbach, H. Ichii, J. Bania, V. Khosrawipour, Evaluating the massive
645 underreporting and undertesting of COVID-19 cases in multiple global epicenters. *Pulmonology* (2020),
646 doi:10.1016/j.pulmoe.2020.05.015.

647 6. J. D. Silverman, N. Hupert, A. D. Washburne, Using influenza surveillance networks to estimate state-specific
648 prevalence of SARS-CoV-2 in the United States. *Science Translational Medicine* (2020),
649 doi:10.1126/scitranslmed.abc1126.

650 7. D. Böhning, I. Rocchetti, A. Maruotti, H. Holling, Estimating the undetected infections in the Covid-19
651 outbreak by harnessing capture-recapture methods. *Int. J. Infect. Dis.* **97**, 197–201 (2020).

652 8. Y. H. Baek, J. Um, K. J. C. Antigua, J.-H. Park, Y. Kim, S. Oh, Y. Kim, W.-S. Choi, S. G. Kim, J. H. Jeong, B.
653 S. Chin, H. D. G. Nicolas, J.-Y. Ahn, K. S. Shin, Y. K. Choi, J.-S. Park, M.-S. Song, Development of a reverse
654 transcription-loop-mediated isothermal amplification as a rapid early-detection method for novel SARS-CoV-2.
655 *Emerg Microbes Infect*. **9**, 998–1007 (2020).

656 9. L. Leo, Mylab gets commercial approval from ICMR for Covid-19 antigen rapid testing kit. *Livemint* (2020),
657 (available at https://www.livemint.com/news/india/mylab-gets-commercial-approval-from-icmr-for-covid-19-
658 antigen-rapid-testing-kit-11595434040321.html).

659 10. S. Dey, Coronavirus testing: Rapid antigen tests now make up nearly half of daily checks | India News - Times
660 of India. *The Times of India*, (available at https://timesofindia.indiatimes.com/india/rapid-antigen-tests-now-
661 make-up-nearly-half-of-daily-checks/articleshow/77340459.cms).

662 11. C. B. F. Vogels, A. F. Brito, A. L. Wyllie, J. R. Fauver, I. M. Ott, C. C. Kalinich, M. E. Petrone, A. Casanovas-
663 Massana, M. Catherine Muenker, A. J. Moore, J. Klein, P. Lu, A. Lu-Culligan, X. Jiang, D. J. Kim, E. Kudo, T.
664 Mao, M. Moriyama, J. E. Oh, A. Park, J. Silva, E. Song, T. Takahashi, M. Taura, M. Tokuyama, A.
665 Venkataraman, O.-E. Weizman, P. Wong, Y. Yang, N. R. Cheemarla, E. B. White, S. Lapidus, R. Earnest, B.
666 Geng, P. Vijayakumar, C. Odio, J. Fournier, S. Bermejo, S. Farhadian, C. S. Dela Cruz, A. Iwasaki, A. I. Ko,
667 M. L. Landry, E. F. Foxman, N. D. Grubaugh, Analytical sensitivity and efficiency comparisons of SARS-
668 CoV-2 RT-qPCR primer-probe sets. *Nat Microbiol* (2020), doi:10.1038/s41564-020-0761-6.

669 12. D. B. Larremore, B. Wilder, E. Lester, S. Shehata, J. M. Burke, J. A. Hay, M. Tambe, M. J. Mina, R. Parker,
670 Test sensitivity is secondary to frequency and turnaround time for COVID-19 surveillance. *medRxiv* (2020),
671 doi:10.1101/2020.06.22.20136309.

672 13. Z. Shen, F. Ning, W. Zhou, X. He, C. Lin, D. P. Chin, Z. Zhu, A. Schuchat, Superspreading SARS events,
673 Beijing, 2003. *Emerging Infect. Dis.* **10**, 256–260 (2004).

674 14. J. S. M. Peiris, C. M. Chu, V. C. C. Cheng, K. S. Chan, I. F. N. Hung, L. L. M. Poon, K. I. Law, B. S. F. Tang,
675 T. Y. W. Hon, C. S. Chan, K. H. Chan, J. S. C. Ng, B. J. Zheng, W. L. Ng, R. W. M. Lai, Y. Guan, K. Y. Yuen,
676 HKU/UCH SARS Study Group, Clinical progression and viral load in a community outbreak of coronavirus-
677 associated SARS pneumonia: a prospective study. *Lancet*. **361**, 1767–1772 (2003).

678 15. X. He, E. H. Y. Lau, P. Wu, X. Deng, J. Wang, X. Hao, Y. C. Lau, J. Y. Wong, Y. Guan, X. Tan, X. Mo, Y.
679 Chen, B. Liao, W. Chen, F. Hu, Q. Zhang, M. Zhong, Y. Wu, L. Zhao, F. Zhang, B. J. Cowling, F. Li, G. M.
680 Leung, Temporal dynamics in viral shedding and transmissibility of COVID-19. *Nat. Med.* **26**, 672–675 (2020).

16. J. Bullard, K. Dust, D. Funk, J. E. Strong, D. Alexander, L. Garnett, C. Boodman, A. Bello, A. Hedley, Z. Schiffman, K. Doan, N. Bastien, Y. Li, P. G. Van Caeseele, G. Poliquin, Predicting infectious SARS-CoV-2 from diagnostic samples. *Clin. Infect. Dis.* (2020), doi:10.1093/cid/ciaa638.

17. G. Giordano, F. Blanchini, R. Bruno, P. Colaneri, A. Di Filippo, A. Di Matteo, M. Colaneri, Modelling the COVID-19 epidemic and implementation of population-wide interventions in Italy. *Nat. Med.* **26**, 855–860 (2020).

18. S. Choi, M. Ki, Estimating the reproductive number and the outbreak size of COVID-19 in Korea. *Epidemiol Health*. **42**, e2020011 (2020).

19. Y. Y. Wei, Z. Z. Lu, Z. C. Du, Z. J. Zhang, Y. Zhao, S. P. Shen, B. Wang, Y. T. Hao, F. Chen, [Fitting and forecasting the trend of COVID-19 by SEIR(+CAQ) dynamic model]. *Zhonghua Liu Xing Bing Xue Za Zhi*. **41**, 470–475 (2020).

20. Z. Yang, Z. Zeng, K. Wang, S.-S. Wong, W. Liang, M. Zanin, P. Liu, X. Cao, Z. Gao, Z. Mai, J. Liang, X. Liu, S. Li, Y. Li, F. Ye, W. Guan, Y. Yang, F. Li, S. Luo, Y. Xie, B. Liu, Z. Wang, S. Zhang, Y. Wang, N. Zhong, J. He, Modified SEIR and AI prediction of the epidemics trend of COVID-19 in China under public health interventions. *J Thorac Dis*. **12**, 165–174 (2020).

21. S. Cao, P. Feng, P. Shi, [Study on the epidemic development of COVID-19 in Hubei province by a modified SEIR model]. *Zhejiang Da Xue Xue Bao Yi Xue Ban*. **49**, 178–184 (2020).

22. R. Huang, M. Liu, Y. Ding, Spatial-temporal distribution of COVID-19 in China and its prediction: A data-driven modeling analysis. *J Infect Dev Ctries*. **14**, 246–253 (2020).

23. A. Godio, F. Pace, A. Vergnano, SEIR Modeling of the Italian Epidemic of SARS-CoV-2 Using Computational Swarm Intelligence. *Int J Environ Res Public Health*. **17** (2020), doi:10.3390/ijerph17103535.

24. M. Gatto, E. Bertuzzo, L. Mari, S. Miccoli, L. Carraro, R. Casagrandi, A. Rinaldo, Spread and dynamics of the COVID-19 epidemic in Italy: Effects of emergency containment measures. *Proc. Natl. Acad. Sci. U.S.A.* **117**, 10484–10491 (2020).

705 25. C. Hou, J. Chen, Y. Zhou, L. Hua, J. Yuan, S. He, Y. Guo, S. Zhang, Q. Jia, C. Zhao, J. Zhang, G. Xu, E. Jia,
706 The effectiveness of quarantine of Wuhan city against the Corona Virus Disease 2019 (COVID-19): A well-
707 mixed SEIR model analysis. *J. Med. Virol.* **92**, 841–848 (2020).

708 26. T. Zhou, Q. Liu, Z. Yang, J. Liao, K. Yang, W. Bai, X. Lu, W. Zhang, Preliminary prediction of the basic
709 reproduction number of the Wuhan novel coronavirus 2019-nCoV. *J Evid Based Med*. **13**, 3–7 (2020).

710 27. C. Reno, J. Lenzi, A. Navarra, E. Barelli, D. Gori, A. Lanza, R. Valentini, B. Tang, M. P. Fantini, Forecasting
711 COVID-19-Associated Hospitalizations under Different Levels of Social Distancing in Lombardy and Emilia-
712 Romagna, Northern Italy: Results from an Extended SEIR Compartmental Model. *J Clin Med*. **9** (2020),
713 doi:10.3390/jcm9051492.

714 28. F. Yu, L. Yan, N. Wang, S. Yang, L. Wang, Y. Tang, G. Gao, S. Wang, C. Ma, R. Xie, F. Wang, C. Tan, L.
715 Zhu, Y. Guo, F. Zhang, Quantitative Detection and Viral Load Analysis of SARS-CoV-2 in Infected Patients.
716 *Clin. Infect. Dis.* **71**, 793–798 (2020).

717 29. S. N. Rao, D. Manissero, V. R. Steele, J. Pareja, A Narrative Systematic Review of the Clinical Utility of Cycle
718 Threshold Values in the Context of COVID-19. *Infect Dis Ther*, 1–14 (2020).

719 30. J. Alizargar, Risk of reactivation or reinfection of novel coronavirus (COVID-19). *J. Formos. Med. Assoc.* **119**,
720 1123 (2020).

721 31. D. Batisse, N. Benech, E. Botelho-Nevers, K. Bouiller, R. Collarino, A. Conrad, L. Gallay, F. Goehringer, M.
722 Gousseff, D. C. Joseph, A. Lemaignen, F.-X. Lescure, B. Levy, M. Mahevas, P. Penot, B. Pozzetto, D. Salmon,
723 D. Slama, N. Vignier, B. Wyplosz, Clinical recurrences of COVID-19 symptoms after recovery: viral relapse,
724 reinfection or inflammatory rebound? *J. Infect.* (2020), doi:10.1016/j.jinf.2020.06.073.

725 32. W. Deng, L. Bao, J. Liu, C. Xiao, J. Liu, J. Xue, Q. Lv, F. Qi, H. Gao, P. Yu, Y. Xu, Y. Qu, F. Li, Z. Xiang, H.
726 Yu, S. Gong, M. Liu, G. Wang, S. Wang, Z. Song, Y. Liu, W. Zhao, Y. Han, L. Zhao, X. Liu, Q. Wei, C. Qin,
727 Primary exposure to SARS-CoV-2 protects against reinfection in rhesus macaques. *Science* (2020),
728 doi:10.1126/science.abc5343.

33. M. Ota, Will we see protection or reinfection in COVID-19? *Nat. Rev. Immunol.* **20**, 351 (2020).

34. A. Victor Okhuese, Estimation of the Probability of Reinfection With COVID-19 by the Susceptible-Exposed-Infectious-Removed-Undetectable-Susceptible Model. *JMIR Public Health Surveill*. **6**, e19097 (2020).

35. Y. Gu, COVID-19 Projections Using Machine Learning. *COVID-19 Projections Using Machine Learning*, (available at https://covid19-projections.com/).

36. D. Stadlbauer, J. Tan, K. Jiang, M. Hernandez, S. Fabre, F. Amanat, C. Teo, G. A. Arunkumar, M. McMahon, J. Jhang, M. Nowak, V. Simon, E. Sordillo, H. van Bakel, F. Krammer, *medRxiv*, in press, doi:10.1101/2020.06.28.20142190.

37. A. Goodnough, M. D. Shear, The U.S.'s Slow Start to Coronavirus Testing: A Timeline. *The New York Times* (2020), (available at https://www.nytimes.com/2020/03/28/us/coronavirus-testing-timeline.html).

38. M. D. Shear, A. Goodnough, S. Kaplan, S. Fink, K. Thomas, N. Weiland, The Lost Month: How a Failure to Test Blinded the U.S. to Covid-19. *The New York Times* (2020), (available at https://www.nytimes.com/2020/03/28/us/testing-coronavirus-pandemic.html).

39. S. Kaplan, K. Thomas, Despite Promises, Testing Delays Leave Americans 'Flying Blind.' *The New York Times* (2020), (available at https://www.nytimes.com/2020/04/06/health/coronavirus-testing-us.html).

40. W. M. de Souza, L. F. Buss, D. da S. Candido, J.-P. Carrera, S. Li, A. E. Zarebski, R. H. M. Pereira, C. A. Prete, A. A. de Souza-Santos, K. V. Parag, M. C. T. D. Belotti, M. F. Vincenti-Gonzalez, J. Messina, F. C. da Silva Sales, P. dos S. Andrade, V. H. Nascimento, F. Ghilardi, L. Abade, B. Gutierrez, M. U. G. Kraemer, C. K. V. Braga, R. S. Aguiar, N. Alexander, P. Mayaud, O. J. Brady, I. Marcilio, N. Gouveia, G. Li, A. Tami, S. B. de Oliveira, V. B. G. Porto, F. Ganem, W. A. F. de Almeida, F. F. S. T. Fantinato, E. M. Macário, W. K. de Oliveira, M. L. Nogueira, O. G. Pybus, C.-H. Wu, J. Croda, E. C. Sabino, N. R. Faria, Epidemiological and clinical characteristics of the COVID-19 epidemic in Brazil. *Nature Human Behaviour*. **4**, 856–865 (2020).

41. S. Mervosh, M. Fernandez, 'It's Like Having No Testing': Coronavirus Test Results Are Still Delayed. *The New York Times* (2020), (available at https://www.nytimes.com/2020/08/04/us/virus-testing-delays.html).

753 42. K. Gostic, A. C. Gomez, R. O. Mummah, A. J. Kucharski, J. O. Lloyd-Smith, Estimated effectiveness of
754 symptom and risk screening to prevent the spread of COVID-19. *eLife*. **9**, e55570 (2020).

755 43. T. Zitek, The Appropriate Use of Testing for COVID-19. *West J Emerg Med*. **21**, 470–472 (2020).

756 44. I. Bosch, H. de Puig, M. Hiley, M. Carré-Camps, F. Perdomo-Celis, C. F. Narváez, D. M. Salgado, D.
757 Senthoor, M. O'Grady, E. Phillips, A. Durbin, D. Fandos, H. Miyazaki, C.-W. Yen, M. Gélvez-Ramírez, R. V.
758 Warke, L. S. Ribeiro, M. M. Teixeira, R. P. Almeida, J. E. Muñóz-Medina, J. E. Ludert, M. L. Nogueira, T. E.
759 Colombo, A. C. B. Terzian, P. T. Bozza, A. S. Calheiros, Y. R. Vieira, G. Barbosa-Lima, A. Vizzoni, J.
760 Cerbino-Neto, F. A. Bozza, T. M. L. Souza, M. R. O. Trugilho, A. M. B. de Filippis, P. C. de Sequeira, E. T. A.
761 Marques, T. Magalhaes, F. J. Díaz, B. N. Restrepo, K. Marín, S. Mattar, D. Olson, E. J. Asturias, M. Lucera, M.
762 Singla, G. R. Medigeshi, N. de Bosch, J. Tam, J. Gómez-Márquez, C. Clavet, L. Villar, K. Hamad-Schifferli, L.
763 Gehrke, Rapid antigen tests for dengue virus serotypes and Zika virus in patient serum. *Sci Transl Med*. **9**
764 (2017), doi:10.1126/scitranslmed.aan1589.

765 45. Massachusetts Department of Public Health, COVID-19 Response Reporting. *Mass.gov*, (available at
766 https://www.mass.gov/info-details/covid-19-response-reporting).

767 46. California Department of Public Health, COVID-19 Cases - California Open Data, (available at
768 https://data.ca.gov/dataset/covid-19-cases).

769 47. California Department of Public Health, COVID-19 Hospital Data - California Open Data, (available at
770 https://data.ca.gov/dataset/covid-19-hospital-data).

771 48. Department of Health and Human Hygiene, COVID-19 Daily Counts of Cases, Hospitalizations, and Deaths |
772 NYC Open Data, (available at https://data.cityofnewyork.us/Health/COVID-19-Daily-Counts-of-Cases-
773 Hospitalizations-an/rc75-m7u3).

774 49. Sao Jose do Rio Preto Public Health Office, "COVID-19 Surveillance Data, Sao Jose do Rio Preto" (Sao Jose
775 do Rio Preto Public Health Office, Sao Jose do Rio Preto, Brazil).

50. New York State Government, Daily Hospitalization Summary by Region. *New York Forward*, (available at https://forward.ny.gov/daily-hospitalization-summary-region).

51. Massachusetts General Hospital Institute for Technology Assessment, COVID-19 Simulator - Methodology, (available at https://www.covid19sim.org/images/docs/COVID-19_simulator_methodology_download_20200507.pdf).

52. CDC, Coronavirus Disease 2019 (COVID-19). *Centers for Disease Control and Prevention* (2020), (available at https://www.cdc.gov/coronavirus/2019-ncov/cases-updates/commercial-lab-surveys.html).

53. SciPy.org — SciPy.org, (available at https://www.scipy.org/).

54. NumPy, (available at https://numpy.org/).

55. Non-Linear Least-Squares Minimization and Curve-Fitting for Python — Non-Linear Least-Squares Minimization and Curve-Fitting for Python, (available at https://lmfit.github.io/lmfit-py/).

56. Matplotlib: Python plotting — Matplotlib 3.3.1 documentation, (available at https://matplotlib.org/).

57. Plotly: The front-end for ML and data science models, (available at https://plotly.com/).

Acknowledgments

General: We thank Professor Lee Gehrke for critical reading of the manuscript.

Funding: The study is funded, in part, by a Bill and Melinda Gates Foundation Award (INV-017872) to E25Bio, Inc. EN is funded by Tufts University DISC Seed Grant. MLN is supported by a FAPESP grant (#2020/04836-0) and is a CNPq Research Fellow. AFV is supported by a FAPESP Fellow grant (#18/17647-0). GRFC is supported by a FAPESP

Fellow grant (#20/07419-0). BHGAM is supported by a FAPESP Scholarship (#19/06572-2). The funders had no role in the design of the study; in the collection, analyses, or interpretation of data; in the writing of the manuscript, or in the decision to publish the results.

Author contributions: Conceptualization: BBH. Formal analysis: BN, AB, AR, MB, NS, ARG, AV, GCDS, TMILDS, BHGAM, MMM, GRFC, FQ, AFNR, MLG, ENN, IB, BBH. Funding acquisition: IB, BBH. Investigation: BN, AB, AR, MB, NS, ARG, AV, GCDS, TMILDS, BHGAM, MMM, GRFC, FQ, AFNR, MLG, ENN, IB, BBH. Methodology: BN, AB, AR, MB, NS, ARG, AV, GCDS, TMILDS, BHGAM, MMM, GRFC, FQ, AFNR, MLG, ENN, IB, BBH. Project administration: MLN, IB, BBH. Resources: MLN, IB, BBH. Supervision: MB, MLN, ENN, IB, BBH. Validation: BN, AB, AR, MB, ENN, BBH. Visualization: BN, AB, AR, MB, AV, ENN, BBH. Writing—original draft: AR, BBH. Writing—review and editing: BN, AB, AR, MB, NS, ARG, AV, GCDS, TMILDS, BHGAM, MMM, GRFC, FQ, AFNR, MLG, ENN, IB, BBH.

Competing interests: BN, AB, AR, MB, NS, AG, IB, and BBH are employed by or affiliated with E25Bio Inc. (www.e25bio.com), a company that develops diagnostics for epidemic viruses.

821 **Figures and Tables**

822

823 **TABLES**

824

825 **Table 1. Clinical validation summary for the direct antigen rapid test (DART) for SARS-**

826 **CoV-2 nucleocapsid protein evaluated using 190 retrospectively collected patient nasal**

827 **swab specimens.**

828

829

All Data Summary								
		qRT-PCR (gene average)					95% Confidence Interval	
		+	-	Total	Sensitivity	80.0%	76.1%	83.9%
DART (nucleocapsid protein)	+	80	8	88	Specificity	91.1%	88.2%	94.0%
	-	20	82	102	Positive Predictive Value	90.9%	87.9%	93.9%
	Total	100	90	190	Negative Predictive Value	80.4%	76.6%	84.2%
					Prevalence	52.6%	47.8%	57.5%
					Overall Agreement	85.3%	82.8%	87.8%

830

831

832

833

834

835 **Table 2. Clinical validation summary for the SARS-CoV-2 direct antigen rapid test**

836 **(DART) for SARS-SoC-2 spike glycoprotein evaluated using 121 retrospectively collected**

837 **patient nasopharyngeal swab specimens.**

838

839

All Data Summary								
		qRT-PCR (gene average)					95% Confidence Interval	
		+	-	Total	Sensitivity	84.7%	80.6%	88.9%
DART (spike glycoprotein)	+	61	7	68	Specificity	85.7%	80.8%	90.6%
	-	11	42	53	Positive Predictive Value	89.7%	86.2%	93.2%
	Total	72	49	121	Negative Predictive Value	79.2%	73.6%	84.9%
					Prevalence	59.5%	53.9%	65.1%
					Overall Agreement	85.1%	82.0%	88.3%

840

841

842

843

844

845

846

847

848

849

850

Table 3. Details of parameter values used for *SIDHRE-Q* Model.

Parameter	Details & Statistics			
α	α is the probability that an interaction between an undetected infected person and an uninfected person results in a new infection, divided by the average number of uninfected people an undetected infected person comes into contact with on a given day. α is estimated from the data.		Mean	St. Dev.
		MA	0.088	0.051
		LA	0.090	0.034
		NYC	0.067	0.042
		SJRP	0.121	0.042
η	η is the probability that an interaction between an infected person and an uninfected person results in a new infection, divided by the average number of uninfected people a detected infected person comes into contact with on a given day. $\eta = 0.01 \cdot \alpha$ The constant relating η, α accounts for a small but nonzero transmission due to the quarantined (detected) infected population. This value was chosen to be small, assuming a quarantined individual will only infect others with low probability.			
ν	ν is the probability that a symptomatic undetected individual is diagnosed on a given day. ν is estimated from the data. ν is multiplied by sensitivity (assume benchmark sensitivity 100% for PCR, as used when fitting).		Mean	St. Dev.
		MA	0.006	0.005
		LA	0.011	0.006
		NYC	0.0056	0.002
		SJRP	0.015	0.007
ϵ	ϵ is the probability that an asymptomatic undetected infected individual is diagnosed on a given day. $\epsilon = 0$ while fitting (during PCR symptomatic testing). ϵ =(sensitivity/days between tests) when the rapid testing strategy is activated.			
λ	λ is the probability that an undetected infected individual transitions to the recovered state on a given day. $\lambda =$			

<table>
<tr><td></td><td colspan="4">$1/14$, or the inverse of average recovery time (51).</td></tr>
<tr><td>μ</td><td rowspan="5">μ is the probability that an infected individual develops severe symptoms on a given day and transitions into the hospitalized state. The flow from D to H is assumed to be independent of the ratio I/D, but comes only from the detected infected population, hence why it is multiplied by $(I + D)/D$. μ is estimated from the data.</td><td></td><td>Mean</td><td>St. Dev.</td></tr>
<tr><td></td><td>MA</td><td>0.0013</td><td>9.5e-4</td></tr>
<tr><td></td><td>LA</td><td>0.0016</td><td>2.4e-4</td></tr>
<tr><td></td><td>NYC</td><td>0.0011</td><td>6.6e-4</td></tr>
<tr><td></td><td>SJRP</td><td>0.0018</td><td>8.0e-4</td></tr>
<tr><td>ρ</td><td colspan="4">$\rho$is the probability that a detected infected individual transitions to the recovered state on a given day.

$\rho = 1/14$, or the inverse of the average recovery time (51).</td></tr>
<tr><td>σ</td><td colspan="4">$\sigma$is the probability that a hospitalized individual transitions to the recovered state on a given day. $\sigma = 1/11$, or the inverse of the average recovery time for a hospitalized individual (51).</td></tr>
<tr><td>τ</td><td rowspan="5">τ is the probability that a hospitalized individual expires on a given day. τ is estimated from the data.</td><td></td><td>Mean</td><td>St. Dev.</td></tr>
<tr><td></td><td>MA</td><td>0.034</td><td>0.012</td></tr>
<tr><td></td><td>LA</td><td>0.016</td><td>0.004</td></tr>
<tr><td></td><td>NYC</td><td>0.036</td><td>0.034</td></tr>
<tr><td></td><td>SJRP</td><td>0.032</td><td>0.045</td></tr>
<tr><td>γ</td><td colspan="4">γ is the probability of entering either of the quarantine states on a given day from either the Susceptible or Recovered populations. $\gamma = 0$ while fitting (during PCR symptomatic testing). $\gamma = (1 - \text{specificity}) \times (1/\text{days between tests})$ when the rapid testing strategy is activated.</td></tr>
<tr><td>ψ</td><td colspan="4">$\psi$is the probability that an individual exits quarantine on a given day. $\psi = 1/14$, or the inverse of the quarantine period for fixed length quarantine.</td></tr>
<tr><td>Parameter</td><td colspan="4">Details & Statistics</td></tr>
</table>

α	α is the probability that an interaction between an undetected infected person and an uninfected person results in a new infection, divided by the average number of uninfected people an undetected infected person comes into contact with on a given day. α is estimated from the data.		Mean	St. Dev.
		MA	0.088	0.051
		LA	0.090	0.034
		NYC	0.067	0.042
		SJRP	0.121	0.042
η	η is the probability that an interaction between an infected person and an uninfected person results in a new infection, divided by the average number of uninfected people a detected infected person comes into contact with on a given day. $\eta = 0.01 \cdot \alpha$ The constant relating η, α accounts for a small but nonzero transmission due to the quarantined (detected) infected population. This value was chosen to be small, assuming a quarantined individual will only infect others with low probability.			
ν	ν is the probability that a symptomatic undetected individual is diagnosed on a given day. ν is estimated from the data. ν is multiplied by sensitivity (assume benchmark sensitivity 100% for PCR, as used when fitting).		Mean	St. Dev.
		MA	0.006	0.005
		LA	0.011	0.006
		NYC	0.0056	0.002
		SJRP	0.015	0.007
ϵ	ϵ is the probability that an asymptomatic undetected infected individual is diagnosed on a given day. $\epsilon = 0$ while fitting (during PCR symptomatic testing). $\epsilon =$ (sensitivity/days between tests) when the rapid testing strategy is activated.			
λ	λ is the probability that an undetected infected individual transitions to the recovered state on a given day. $\lambda = 1/14$, or the inverse of average recovery time (*51*).			
μ	μ is the probability that an infected individual develops severe symptoms on a		Mean	St. Dev.
		MA	0.0013	9.5e-4

	given day and transitions into the hospitalized state. The flow from D to H is assumed to be independent of the ratio I/D, but comes only from the detected infected population, hence why it is multiplied by $(I+D)/D$. μ is estimated from the data.	LA	0.0016	2.4e-4
		NYC	0.0011	6.6e-4
		SJRP	0.0018	8.0e-4
ρ	ρ is the probability that a detected infected individual transitions to the recovered state on a given day. $\rho = 1/14$, or the inverse of the average recovery time (*51*).			
σ	σ is the probability that a hospitalized individual transitions to the recovered state on a given day. $\sigma = 1/11$, or the inverse of the average recovery time for a hospitalized individual (*51*).			
τ	τ is the probability that a hospitalized individual expires on a given day. τ is estimated from the data.		Mean	St. Dev.
		MA	0.034	0.012
		LA	0.016	0.004
		NYC	0.036	0.034
		SJRP	0.032	0.045
γ	γ is the probability of entering either of the quarantine states on a given day from either the Susceptible or Recovered populations. $\gamma = 0$ while fitting (during PCR symptomatic testing). $\gamma = (1 - \text{specificity}) \times (1/\text{days between tests})$ when the rapid testing strategy is activated.			
ψ	ψ is the probability that an individual exits quarantine on a given day. $\psi = 1/14$, or the inverse of the quarantine period for fixed length quarantine.			

857 **FIGURES**

858 **Figure 1. Graphical scheme displaying the relationships between the stages of quarantine**
859 **and infection in *SIDHRE-Q* mode**l. **Q-U**, quarantine uninfected; **S**, susceptible (uninfected); **I**,
860 infected undetected (pre-testing and infected); **D**, infected detected (infection diagnosis through
861 testing); **H**, hospitalized (infected with life threatening symptom progression); **R**, recovered
862 (healed); **E**, extinct (dead); and **Q-R**, quarantine recovered (healed but in quarantine by false
863 positive testing).

864

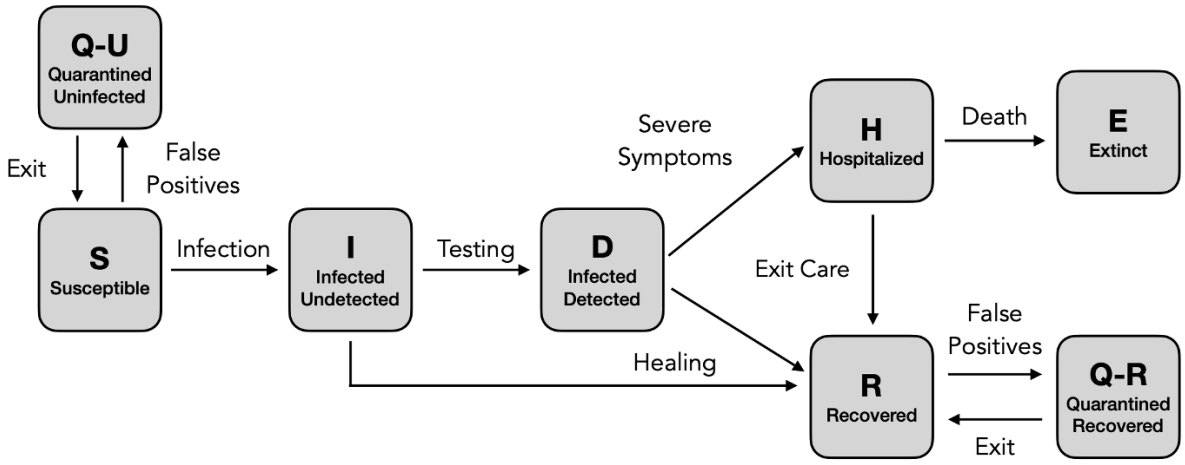

865

866

867

868

869

870

871

872

873

874 **Figure 2. COVID-19 Outcomes in 3 US Regions and Brazil as a result of Frequent Rapid**
875 **Testing Protocol using the *SIDHRE-Q* Model.** (A) The Cumulative Detected Infected,
876 Hospitalized, Deceased, Active Infections, Recovered, and Quarantined are modeled over 105
877 days (top to bottom) using reported data from 4 global regions: Massachusetts, Los Angeles,
878 New York City, and São José do Rio Preto in Brazil (left to right). The COVID-19 population
879 spread and outcomes are modeled under a Rapid Testing Protocol (sensitivity 80%, specificity
880 90%) with variable testing frequencies ranging from 1-21 days between tests. This protocol is
881 compared to a symptom-based Rapid Testing protocol and a symptom-based PCR protocol. (B)
882 Effect of Rapid Testing Protocol under variable testing sensitivities (30%-90%) and increasing
883 frequency under the *SIDHRE-Q* Model. The Cumulative Infections, Maximum Simultaneously
884 Hospitalized, and Deceased populations are modeled for Massachusetts, Los Angeles, New York
885 City, and São José do Rio Preto in Brazil with a 90% test specificity.
886
887
888
889
890
891
892
893
894
895
896

(A)

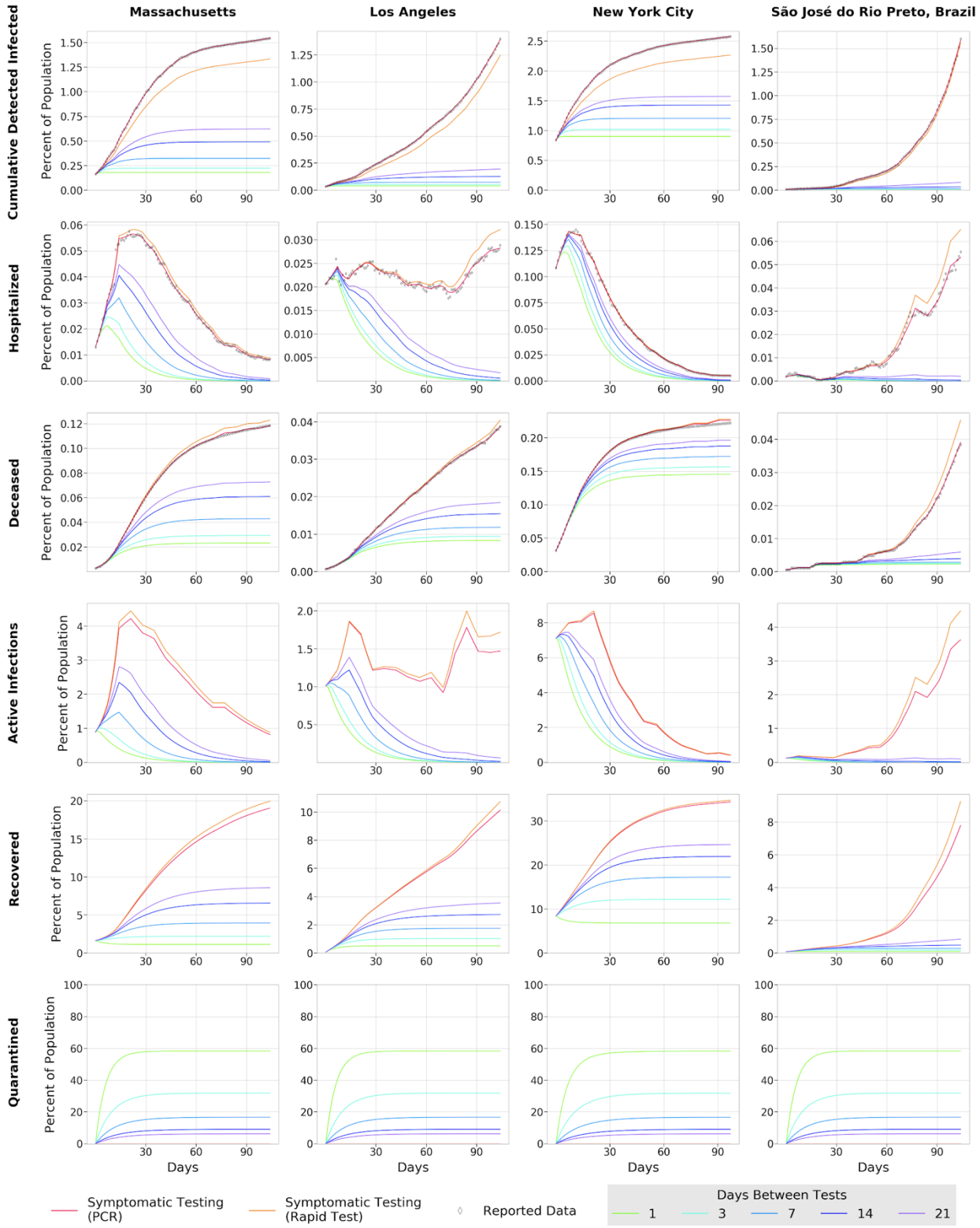

Sensitivity: 80.0% Specificity: 90.0%

(B)

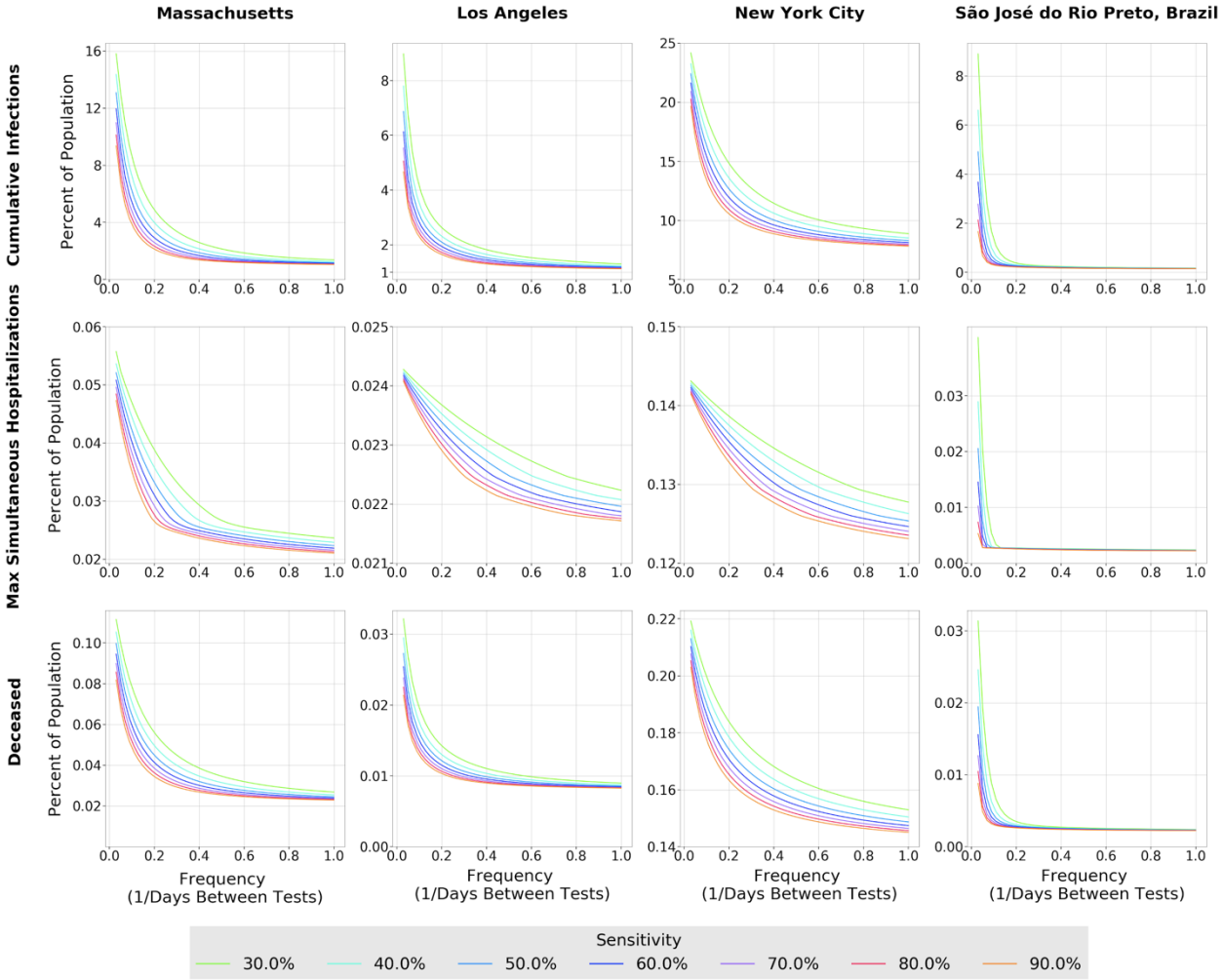

Specificity: 90.0%
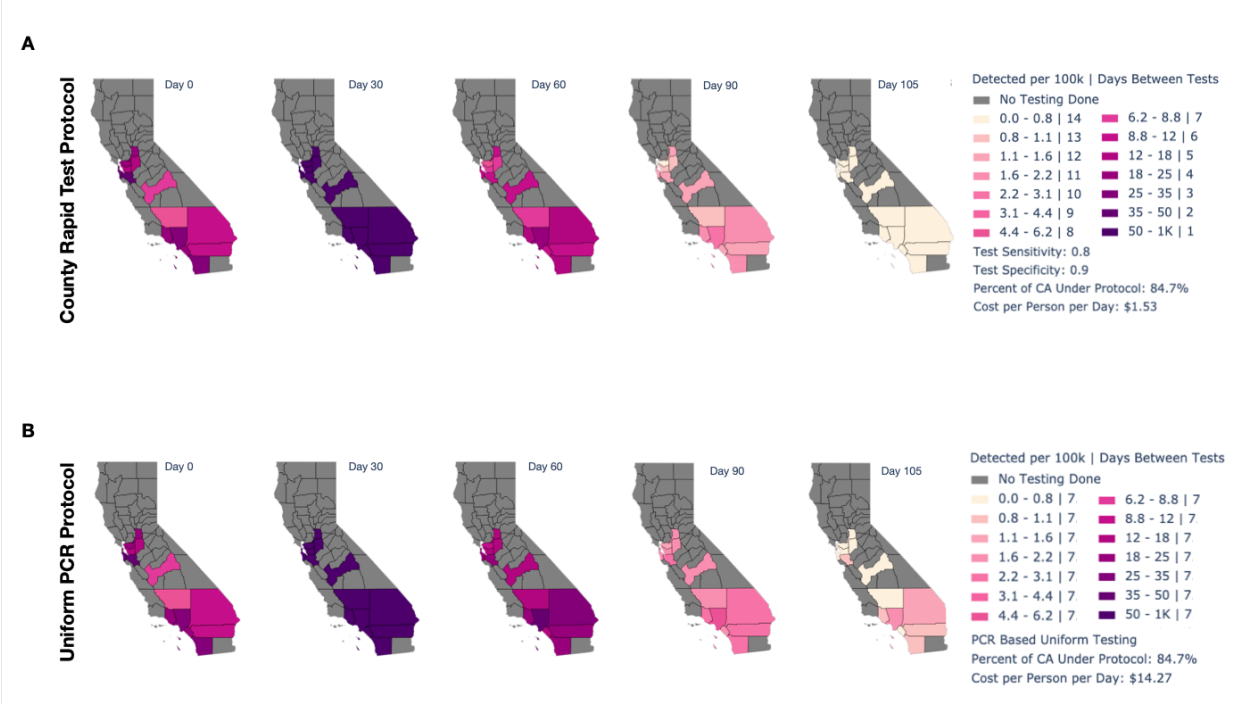
Figure 3. Effect of County Based Rapid Test Protocol (A) and Uniform PCR Protocol (B) on active infected detected population over time in California (CA). The legend denotes the thresholds at which testing frequency is determined, the testing frequencies, the percent of CA population under the strategy, and the cost per person per day.